3D Interconnected Macro-mesoporous Electrode with Self-assembled NiO nanodots for High-performance Supercapacitor-like Li-ion Battery

Xianfeng Zheng[a], Hongen Wang[a], Chao Wang[a], Zhao Deng[a], Lihua Chen,[a] Yu Li,[a]* Tawfique Hasan[b, c] and Bao-Lian Su[a,d,e,]*

[a]*Laboratory of Living Materials at the State Key Laboratory of Advanced Technology for Materials Synthesis and Processing, Wuhan University of Technology, 122 Luoshi Road, 430070 Wuhan, Hubei, China; Email: yu.li@whut.edu.cn and baoliansu@whut.edu.cn*

[b]*Cambridge Graphene Centre, University of Cambridge, Cambridge, CB3 0FA, UK*

[c]*Nanoscience Centre, University of Cambridge, Cambridge CB3 0FF, UK*

[d]*Laboratory of Inorganic Materials Chemistry (CMI), University of Namur, 61 rue de Bruxelles, B-5000 Namur, Belgium; E-mail: bao-lian.su@unamur.be*

[e]*Department of Chemistry and Clare Hall, University of Cambridge, Cambridge CB2 1EW, UK; E-mail: bls26@cam.ac.uk*

Abstract

We report a binder-free three-dimensional (3D) macro-mesoporous electrode architecture via self-assembly of 3 nm NiO nanodots on macroporous nickel foam for high performance supercapacitor-like lithium battery. This electrode architecture provides a hierarchically 3D macro-mesoporous electrolyte-filled network that simultaneously enables rapid ion transfer and ultra-short solid-phase ion diffusion. Benefitting from the structural superiority owing to the interconnected porous hierarchy, the electrode exhibits supercapacitor-like high rate capabilities with high lithium battery capacities during the discharge-charge process: a very high capacity of 518 mA h g^{-1} at an ultrahigh current density of 50 A g^{-1}. It exceeds at least ~10 times than that of the state-of-art graphite anode, which shows only ~50 mA h g^{-1} at ~2-3 A g^{-1} as anode for Li-ion battery. The preparation method to 3D interconnected hierarchically macro-mesoporous electrode, presented here can provide an efficient new binder free-electrode technique towards the development of high-performance supercapacitor-like Li-ion batteries.

Keywords: NiO, Nanodots, Self-assembly, Supercapacitor, Lithium-ion Battery

Introduction

In recent years, the search for high-performance electrochemical energy storage devices have drawn significant attention due to the fossil-fuel crisis and ever-increasing demand for renewable energy in the modern society. [1] Indeed, storing high-density energy at high charge-discharge rate is strongly desired by the technology companies and consumers alike. [2, 3] Conventionally, electrochemical supercapacitors deliver high power density (1-10 kW kg^{-1}) but low energy density (1-10 Wh kg^{-1}) as they involve non-solid state ion diffusion and only store energy by surface adsorption reactions of charged species on an electrode material. [4-6] By storing charge in the bulk of a material via conversion or alloying-dealloying reaction, Li-ion batteries (LIBs) offer high energy density (100 Wh kg^{-1}) but low power density (0.1 kW kg^{-1}) due to the poor rate capabilities of electrodes suffering from formidable diffusion kinetic problems. [4, 7] A Li-ion energy-storage device that combines the high capacity of LIBs with the high-rate performance characteristics of supercapacitors, namely supercapacitor-like Li-ion battery, can significantly advance the technology involving electric and plug-in hybrid electric vehicles and storage for wind and solar energy.

Such a Li-ion battery would generally require three-dimensional (3D) electrode architecture for providing rapid ion transfer in electrolyte-filled porous networks and excellent electron conduction. [3] Superior to the traditional copper foil (CF) electrode and irregular porous carbon-black, conductive metal foam electrodes with a 3D interconnected macroporous network offer a binder-free electrode configuration and have recently proven to be particularly promising. [3, 8-11] For solid-state Li-ion diffusion, the mean diffusion time τ_{eq} for diffusion is proportional to the square of the characteristic dimensions of active materials L by the following formula, $\tau_{eq} = L^2/2D$, where D is the diffusion coefficient. [3, 12, 13] This means that reducing the particle-size should very effectively boost the rate capability of batteries. In this context, well-defined, nanosized active materials with mesopores for electrolyte access are widely sought, but are currently restricted to a relatively large particle-size of ~50 nm. [12-15] Thus far, only modest rate-performance improvements (0.1-2 A g^{-1}) have been archived in these anode materials based on transition-metal oxides. [10, 11, 14] Previously investigated routes include chemical treatment at high-temperature and solution growth in hydrothermal reaction, which can be used to produce coating of compatible materials on macroporous nickel foam (NF), such as NiP_2, Ni_3S_2, Co_3O_4 and CoO. [10, 14-16]

However, further reducing the particle-size has been proved to be very challenging. [10, 14-17] As an alternative route, self-assembling pre-synthesized nanoparticles on NF could be a more feasible pathway, because their sizes are readily tunable during the solution-phase synthesis procedure. [18-22] Among the transition metal oxides, nickel oxide (NiO) is a very promising anode material due to its high theoretical capacity (718 mA h g^{-1} for $2Li^+$ per NiO) and good chemical compatibility with NF substrate. [23] Based on the above considerations, self-assembling ultra-small NiO nanoparticles on macroporous NF to fabricate a 3D interconnected macro-mesoporous NiO electrode is thus expected to be very suitable for high performance supercapacitor-like Li-ion battery.

Herein, we report a binder-free electrode architecture via self-assembling electrolytically active 3 nm NiO nanodots to form uniform mesopores on macroporous NF. Such electrode architecture provides a hierarchically 3D interconnected macro-mesoporous electrolyte-filled network, which simultaneously enables rapid ion transfer in electrolyte and ultra-short ion diffusion length in solid-phase. Benefitting from the structural superiority, the 3nm NiO/NF exhibits supercapacitor-like rate capabilities while maintaining high battery capacities during charge-discharge process. In particular, it displays superior charge-discharge stability and ultrahigh rate capability with a capacity of 518 mA h g^{-1} at 50 A g^{-1}. The 3D interconnected macro-mesoporous architecture, facilitated by the self-assembled 3 nm NiO nanodots on NF presented here is a significant step towards the development of high-performance supercapacitor-like Li-ion batteries.

Materials and synthesis

Materials synthesis and self-assembly

Nickel (acetylacetonate)$_2$ (Ni(acac)$_2$, 99%, Aldrich), oleylamine (96%, Aldrich), ethanol and hexane are used as received. For synthesizing 3 nm NiO, a mixture of oleylamine (8 g) and Ni(acac)$_2$ (1 g) is heated to 100 °C with magnetically stirring under a flow of O_2. The utilization of oxygen atmosphere can ensure the formation of NiO. The solution is heated to 200 °C quickly and kept at this temperature for 30 min. After cooling to room temperature naturally, excess ethanol is added to the solution to induce precipitation, which is then collected via centrifugation. The NiO

nano-dots are repeatedly washed, isolated and dried, and are finally dispersed in hexane to form a dispersion. Residual amines are removed via ethanol wash, as verified by FTIR spectroscopy. The 30 nm NiO nanoparticles are prepared by seed-mediated growth. oleylamine (8 g) and $Ni(acac)_2$ (1.04 g) are mixed and magnetically stirred 100 °C under oxygen atmosphere. 90 mg of 3 nm NiO nanodots dispersed in hexane is added to the hot solution as seed. The mixture is rapidly heated to 200 °C and kept at this temperature for 30 min. This produces a hexane dispersion of 30 nm NiO nanoparticles. For the self-assembly of NiO nanodots/nanoparticles, the nickel foam (NF) and the copper foil (CF) are separately immersed in 1.5 mg/mL NiO nanodot/nanoparticle hexane dispersion. During the hexane evaporation, the NiO nanoparticles are self-assembled on to NF or CF. After degassing at 250 °C under vacuum, 3 nm NiO/NF (mass loading: 3.6 mg cm^{-2}), 30 nm NiO/NF (mass loading: 3.7 mg cm^{-2}) and 3 nm NiO/CF (mass loading: 3.4 mg cm^{-2}) are obtained. Only one side of the samples is in direct contact with the NiO suspension while the other side is protected using sticky tape.

Characterizations

The TEM images are acquired using a JEM-2100F with 200 kV acceleration voltage. The SEM images are taken using a Hitachi S-4800. The XRD pattern is obtained using a Bruker D8 Advance diffractometer equipped with a Cu K_a rotating anode source. The pore-size distribution is acquired by a Micromeritics ASAP 2020 porosimeter. The samples are degassed at 120 °C for 12 h before measurement. The mesopore size is calculated using the Barrett-Joyner-Halenda (BJH) model. The surface area is obtained by Brunauer-Emmett-Teller (BET) method.

Electrochemical measurement

The electrochemical measurements of electrodes for supercapacitor are performed in a three electrode electrochemical cell at room temperature using 6 M KOH as the electrolyte. The as-prepared 3 nm NiO/NF acted directly as the working electrode. A Pt plate and Ag/AgCl are used as the counter electrode and the reference electrode, respectively. All potentials are referred to the reference electrode. The weight-specific capacitance [F g^{-1}] and current rate [A g^{-1}] are calculated based on the mass of NiO. The electrochemical performance of electrodes for Li-ion battery is evaluated via a CR2032-tpye coin cell on a LAND (CT2001A) multichannel battery test system. Batteries are assembled using 3 nm NiO/NF as the working electrode, 1 M solution of $LiPF_6$ in

ethylene carbon (EC)/diethyl carbonate (DEC) (1:1, in wt %) as electrolyte, and a lithium foil as the counter electrode. Galvanostatic discharge/charge measurements are performed on a CHI 660D in a potential range of 3 V-0.02 V vs Li^+/Li. The specific energy E (W h kg^{-1}) is calculated by the integration of specific capacity and voltage from the discharge curves. The specific power P (W kg^{-1}) is calculated by the product of average voltage and discharge current, where the average voltage is the voltage when the capacity reaching 50% of the final value.

Results and discussions

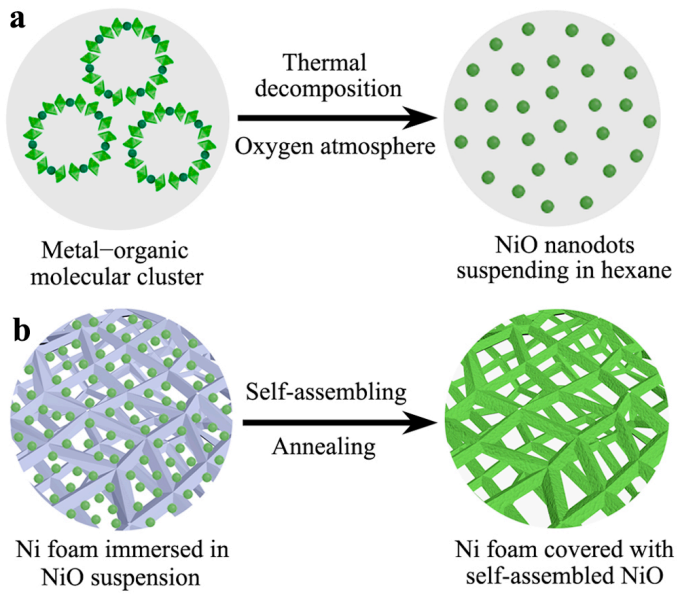

Figure 1. Schematic illustration of (a) the monodisperse 3 nm NiO nanodot preparation and (b) the self-assembly of 3 nm NiO nanodots on macroporous Ni foam.

Figure 1 presents the basic concept underpinning the synthesis and self-assembly of the NiO nanodots. To obtain monodisperse 3 nm NiO nanodots, a modified high-temperature solution-phase technology is used under an oxygen atmosphere (Figure 1a). [20, 21] Conventionally, discrete metal-oxide nanodots are produced by sputtered metal atoms in a cluster gun under oxygen gas chamber. [23, 24] Alternatively, direct synthesis via solution-phase reaction offers a simple, low-cost, scalable and well-controlled production strategy. [20-22, 25] Typically, 1 g nickel(acetylacetonate)$_2$ [Ni(acac)$_2$] and 8 g oleylamine are mixed at 100 °C under an oxygen atmosphere. The resulting solution is rapidly heated to 200 °C and kept at this temperature for 30 min until its color changes from dark-green to yellow-brown, indicating successful synthesis of 3 nm NiO nanodots (Figure S1). The as-synthesized NiO nanodots can be stably dispersed in hexane

without precipitation for several months (Figure S2). Self-assembly of 3 nm NiO nanodots on macroporous NF (designated as 3 nm NiO/NF) or copper foil (designated as 3 nm NiO/CF) is achieved via immersing the substrates into NiO nanodot-hexane dispersions, followed by evaporation at room-temperature and pressure (Figure 1b, see details in experiment section). During evaporation of hexane, NiO nanodots self-assemble via van der Waals forces and tightly adhere to the NF framework after further annealing and degassing. [19, 26] The metallic silver-gray NF becomes dark and the coppery color of CF becomes gray after the self-assembly of NiO nanodots (Figure S3). As a comparison, 30 nm NiO nanoparticles (designated as 30 nm NiO/NF) are also synthesized and self-assembled on NF (See experimental section for details). X-ray diffraction (XRD) patterns on both NF and CF substrates display the three main peaks for the (111), (200) and (220) planes of cubic NiO (JCPDS 78-0643), indicating a self-assembly of randomly orientated 3 nm NiO nanodots (Figure S4).

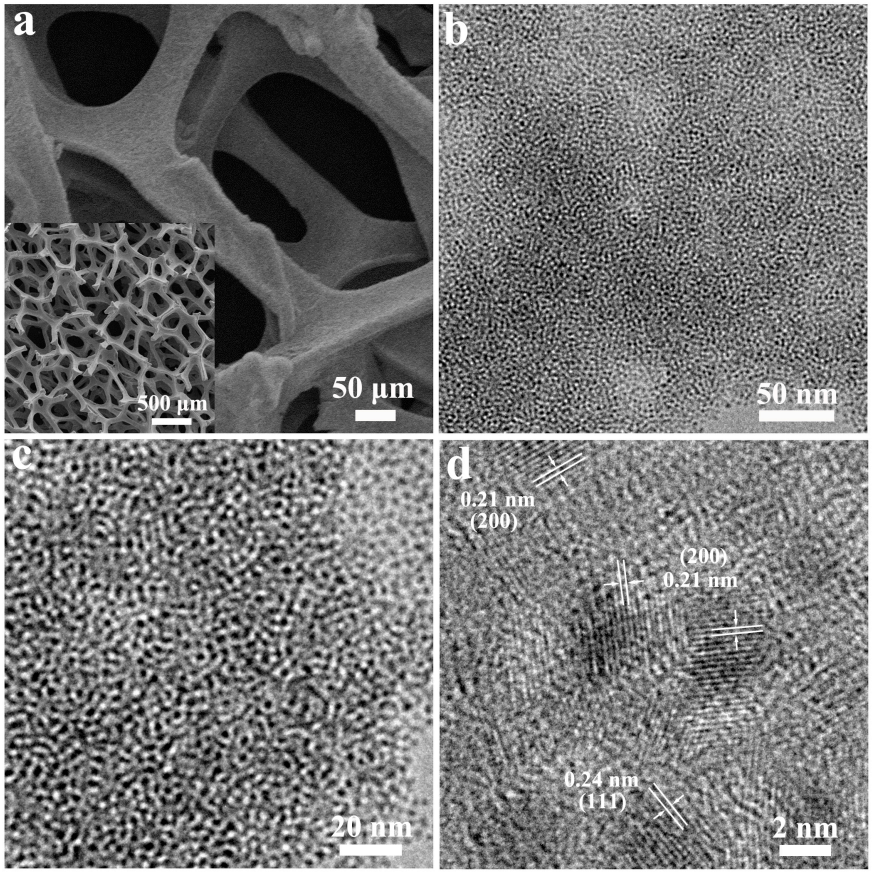

Figure 2. (a) High- and low-magnification (inset) SEM images and (b-d) TEM images at different magnifications of self-assembled 3 nm NiO on NF.

Scanning electron microscopy (SEM) and transmission electron microscopy (TEM) reveal more information on the self-assembled NiO nanodots on the surface of the 3D macroporous NF

(Figure 2). Low-magnification SEM (Figure 2a inset) demonstrates that the 3D interconnected metal backbones of the macroporous networks, which could provide highly efficient path for fast electron transport and high electrochemical utilization of the NiO nanodots. Figure 2a shows that the macroporous skeletons of NF are conformably covered with mesoporous nanostructure assembled by NiO nanodots. SEM images of 3 nm NiO/NF at different magnification are further presented in Figure S5a-c. The TEM image of the NiO nanodots scraped from macroporous NF reveals that a large number of uniform nanodots tightly interconnect with each other to form wormlike channels (Figure 2b) as a result of the randomly-packed self-assembly. These nanochannels between the nanodots clearly show mesopore size ranging from 5 to 10 nm (Figure 2c). The HRTEM lattice fringe image presented in Figure 2d reveals that the size of the NiO nanodots is ~3 nm, indicating a high surface area. Nitrogen adsorption-desorption isotherm further demonstrates a narrow mean size ~7 nm (Figure S5), in agreement with the TEM observation. The BET surface area of 3 nm NiO nanodots is ~268 $m^2 g^{-1}$, much higher than that of the bulk NiO (~3 $m^2 g^{-1}$). As a comparison, 30 nm NiO nanoparticles demonstrate a BET surface area of ~22 $m^2 g^{-1}$ and wormlike nanochannels ~10 nm after self-assembling (Figure S6). This 3D interconnected macro-mesoporous 3 nm NiO/NF nanostructure with high surface area can highly facilitate the access of electrolyte to the active materials. [13, 27]

To show its high rate behavior for supercapacitor-like LIBs, the characteristic rate performance of supercapacitor using our 3 nm NiO/NF electrode is first measured (Figure 3). Cyclic voltammetry (CV) curves exhibit a strong oxidation peak and a sharp reduction peak instead of the rectangular shape. We attribute this to the pseudocapacitance of the NiO nanostructure. The anodic peak ~0.31 V is related to the surface oxidation of NiO to NiOOH ($NiO + OH^- \leftrightarrow NiOOH + e^-$). The cathodic peak at ~0.21 V is its reverse process. [28] The high-power characteristic of supercapacitor can be identified from the voltammetric response at various scan rates from 10 to 100 mV s^{-1}. [16] Obviously, all curves exhibit similar redox shapes and the current density increases with the increasing scan rate. Even at a high scan rate of 100 mV s^{-1}, the CV curve still shows a pair of redox peaks. As the charge storage occurs at the surface layer of the nanostructures immersed in electrolyte, a fast redox action delivering energy at ultra-high rate can be achieved for the electrodes due to interconnected porous network to facilitate highly efficient transfer of the OH^- ions. [4, 27] The specific capacitance values of 30 nm NiO/NF electrode at the current densities of 2,

5, 10, 20 and 50 A g^{-1} are 162, 149, 132, 113 and 90 F g^{-1}, respectively. The effect of particle-size on the performance of NiO nanparticles in supercapacitor was previously studied and showed that the particle size of the NiO nanostructure plays an important role because of the presence of a higher number of active sites for a faradaic reaction. [29] The 3 nm NiO/NF electrode has higher specific surface area for OH^- ion adsorption reaction as seen from the larger area of the enclosed CV curve (Figure S7). Thus, the specific capacitance values of the 3 nm NiO/NF electrode at the same current densities are strongly increased to 856, 823, 806, 778 and 702 F g^{-1}, respectively (Figure 3a), showing as high as 82% capacitance retention. Our capacitances and rate performances are also among the highest in recent literatures reported for NiO materials. [30-34] As supercapacitors only store charges at surface or in thin-layer region of active materials and almost involve no ion diffusion in the bulk of materials, [4] the mesoporous nanostructure self-assembled by 3 nm NiO nanodots on conductive macroporous NF herein demonstrates an outstanding electrode architecture, which could enable rapid ion transfer in the 3D interconnected electrolyte-filled macro-mesoporous networks. After 10,000 cycles, the 3nm NiO/NF electrode exhibits high capacitance retention of 93% at a current density of 2 A g^{-1} (Figure 3b), revealing the long-term charging-discharging stability of these electrodes for electrochemical supercapacitor.

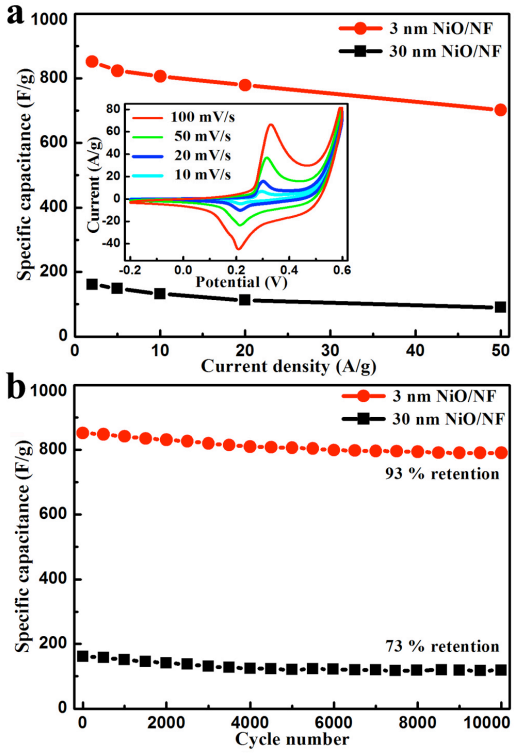

Figure 3. (a) The specific capacitances as a function of current density and (b) cycling stability at 2 A g^{-1} of 3 nm NiO/NF and 30 nm NiO/NF as electrodes for supercapacitor. The inset in (a) shows the cyclic voltammetry curves

of 3 nm NiO/NF at various scan rates.

The Li-storage performances of self-assembled NiO nanodots and nanoparticles on NF substrate as a free-standing binder-free working electrode are next evaluated (Figure 4). The discharge-charge voltage profiles of the 3 nm NiO/NF electrode (Figure 4a inset) exhibit obvious discharge plateau at ~0.7 V and sloping charge plateau at ~1.2 V, responsible for the reversible conversion reaction: $NiO + 2Li^+ + 2e \leftrightarrow Ni + Li_2O$. [23, 35] The 3 nm NiO/NF electrode delivers a discharge capacity of 1045 mA h g^{-1} at the first cycle, which exceeds the theoretical capacity of NiO bulk (718 mA h g^{-1} for $2Li^+$ per NiO). The additional capacity can be attributed to the nanoscale interfacial Li-storage, due to the highly increased surface area of such small-sized nanodots. [36] However, the interfacial Li-storage is partly unstable or irreversible during the cycling. We believe that at the fifth cycle, the capacity decreases to 747 mA h g^{-1} due to this. Still, the 3 nm NiO/NF electrode exhibits a long-life cycling stability up to 1000 cycles with a reversible capacity of 710 mA h g^{-1} at a current density of 1 A g^{-1} (Figure 4a). It is well known that the reversible lithiation and delithiation occurring in the bulk of a material via Li-ions solid-state diffusion can extensively pulverize larger particles into smaller particles of less than ~10 nm, resulting in poor cycle-stability or low capacity retention.[11, 23, 37] However, this pulverizing phenomenon is not observed in our 3 nm NiO/NF electrode. The TEM image (Figure 4a inset) clearly reveals that the nanodot size and the self-assembled mesoporous structure are well maintained after 500 cycles, suggesting the high cycle-stability of 3 nm NiO/NF electrode. [12, 36]

As mentioned above, the characteristic time for Li-ion diffusion through an active material decreases with the square of characteristic size of the active materials. [3, 12, 13] With rapid ion transfer through the entire electrode architecture containing both ultra-short-range solid-state and macro-mesoporous electrolyte-filled networks, considerable Li-storage capacity could be achieved even under ultrahigh rate. [13, 27] The rate capabilities of 3 nm NiO/NF, 30 nm NiO/NF (Figure S6) and 3 nm NiO/CF electrodes (Figure S8) are employed as a comparison. The 3 nm NiO/CF electrode shows no macro-mesoporous networks. Remarkably, the 3 nm NiO/NF electrode exhibits much higher rate capability than both 30 nm NiO/NF and 3 nm NiO/CF electrodes (Figure 4b). The specific capacities of the 3 nm NiO/NF electrode at increasing current densities of 2, 5, 10 and 20 A g^{-1} are 685, 660, 635 and 603 mA h g^{-1}, respectively. The electrochemical impedances for 3 nm

NiO/NF, 30 nm NiO/NF and 3 nm NiO/CF electrodes were also measured as shown in Figure 4c. The arc in the high frequency region corresponds to the charge transfer resistance. The impedance resistances of three samples are ~10 Ω, 14 Ω, and 43 Ω, respectively. And the straight line in the low frequency region is ascribed to the diffusive resistance related to the diffusion of Li-ion in the electrode. The electrochemical impedance spectra (EIS) results verify that the 3 nm NiO/NF electrode architecture exhibits the lowest internal resistance among the three electrodes, showing that the charge transfer throughout the electrode can also be effective enough to accommodate ultrahigh rate due to the closely-packed assembly of 3 nm NiO. [14, 17] The 3 nm NiO/CF presents a much higher impedance resistance, indicating its low conductivity and its low charge transfer capability.

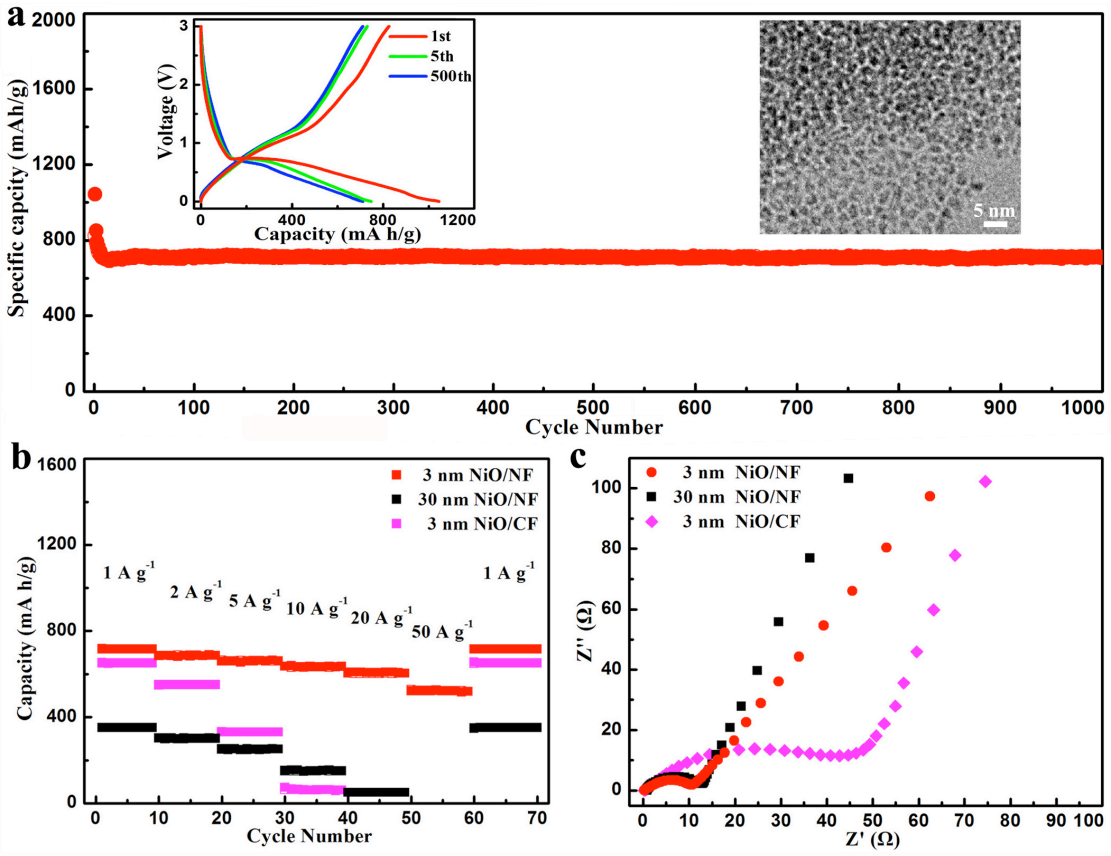

Figure 4. (a) The specific capacity of the 3 nm NiO/NF for Li-ion battery at 1 A g^{-1} for 1000 cycles; (b) Rate capabilities and (c) electrochemical impedances for 3 nm NiO/NF, 30 nm NiO/NF and 3 nm NiO/CF electrodes, respectively. The inset plots in (a) show the 1, 5, and 500 charge-discharge curves. The second inset in (a) is a TEM image, revealing unaltered particle shape, size and mesoporous structure of 3 nm NiO/NF after 500 cycles at 1 A g^{-1}.

The achieved rate performance of 3 nm NiO/NF as the working electrode for Li-ion battery (Figure 5a) is even comparable to that of the supercapacitor (Figure 3a), demonstrating a

supercapacitor-like rate performance. Compared to advanced anode materials recently reported with high rate capability, the capacity retention of 3 nm NiO/NF is 89%, ~2 times higher than those of nitrogen-doped porous carbon and ~8 nm SnO_2 electrodes respectively, where the capacity retention is only 40% and 35% when the current increased from 1 to 10 A g^{-1}. [37, 38] Even at extremely high current density of 50 A g^{-1} (a 50 fold increase in discharge current), the battery with 3 nm NiO/NF electrode delivers a reversible capacity of 518 mA h g^{-1} with 73% capacity retention. Our 3 nm NiO/NF electrode also demonstrate the best rate capability, cycling properties and charge-discharge capacity among the NiO materials reported recently. [39-42] Figure 5b illustrates Ragone plot to describe the relation between energy density and power density of the samples. Our Li-ion battery with 3 nm NiO/NF displays high power density of ~0.7 kW kg^{-1} at an energy density of ~490 Wh kg^{-1}, approaching to the low end for power densities of supercapacitors (1-10 kW kg^{-1}). At higher power density near 1.4, 3.5, 7 and 14 kW kg^{-1}, the energy density is ~480, 460, 440 and 420 Wh kg^{-1}, respectively, bridging the performance gap between normal supercapacitors and batteries. [43] The battery exhibits a higher power density of ~35 kW kg^{-1} with energy density as high as ~360 Wh kg^{-1}, far superior to that of typical supercapacitors (1-10 Wh kg^{-1}) at the same power level. It is also evident that the energy densities achieved here are higher than that of the upper end of traditional Li-ion batteries. The poor performance observed for 3 nm NiO/CF electrode is due to the lack of the meso-macroporous structures of copper foils; showing the importance of the presence of 3D meso-macroporous architecture for rapid charge transfer and ion diffusion. The mass loading of our 3 nm NiO/NF is 3.6 mg cm^{-2}. The capacity is ~710-1045 mA h g^{-1}, which corresponds to a capacity loading as high as ~2.6-3.8 mAh cm^{-2}. This is comparable to the state-of-the-art capacity loading of ~2.0-3.5 mAh/cm^2. Furthermore, the as-obtained reversible capacity of 518 mA h g^{-1} at 50 A g^{-1} exceeds ~10 times than that of the state-of-art graphite anode, which shows only ~50 mA h g^{-1} at ~2-3 A g^{-1} as anode for Li-ion battery. [8] This result would promote further development of higher performance supercapacitor-like Li-ion full-cells in the near future. However, it is very difficult to get high-performace cathode material as standard reference to evaluate the performance of full-cells. Since, similar supercapacitor-like working performance can be obtained from very few of cathode materials, such as nano-sized $LiFePO_4$ and lithiated MnO_2. And these cathode materials possess relatively low energy density of ~20-100 Wh kg^{-1}. [2, 3] These cathode materials need also further optimization and developement. We are working on the full cell

device.

High-performance electrode requires the simultaneous optimization of the primary transfer process during charge and discharge (Figure 5c): (1) ion transfer in the electrolyte, (2) ion diffusion in the electrode, (3) electron conduction in the electrode and current collector. We propose that the high electrochemical performance of 3 nm NiO/CF comes from the unique 3D interconnected macro-mesoporous networks with high surface-area. [3,12,13] We demonstrated that this electrode architecture simultaneously provides excellent electron conduction form metal Ni, rapid ion transfer in electrolyte-filled macro-mesoporous network, and ultra-short solid-phase ion diffusion. We believe that this general material design principle and significant progress we demonstrate here on 3 nm NiO/NF anode material could be used for further development of higher-performance supercapacitor-like Li-ion full-cell in the near future.

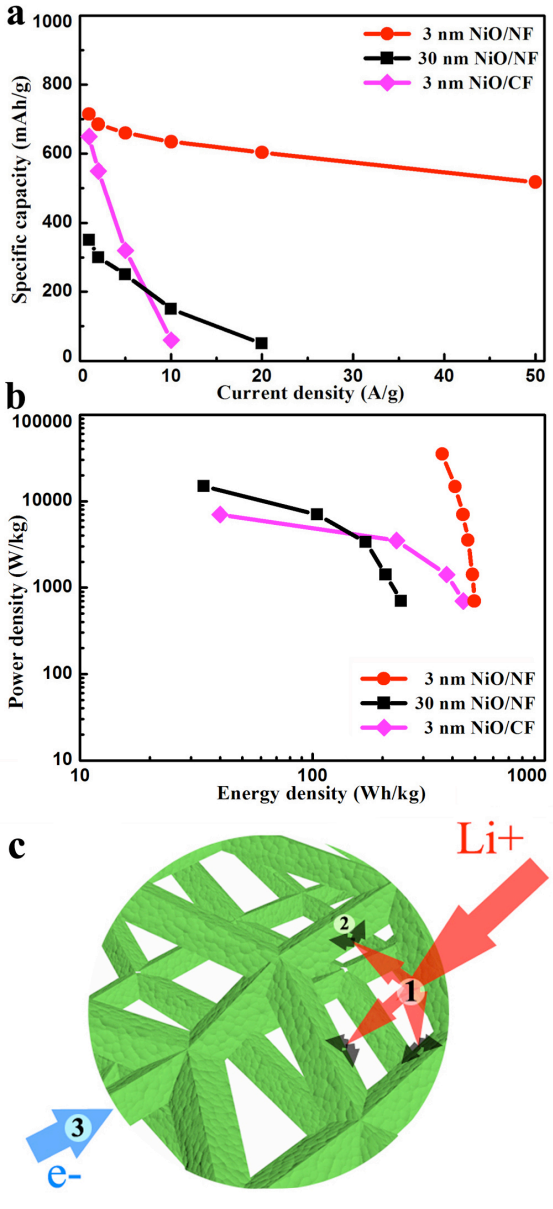

Figure 5. (a) The specific capacity as a function of current density for 3 nm NiO/NF, 30 nm NiO/NF and 3 nm NiO/CF; (b) Ragone plots of the Li-ion batteries using different NiO samples; (c) Illustration of the Li-ion transfer in the electrolyte and electrode, and electron conduction in the electrode for our Li-ion batteries.

Conclusion

We demonstrated a facile approach to fabricate a binder-free macro-mesoporous electrode via self-assembly of 3 nm NiO nanodots on macroporous nickel foam for high-performance supercapacitor-like Li-ion battery. The as-prepared electrode possesses high surface-area and 3D interconnected macro-mesoporous networks, facilitating rapid ion transfer in electrolyte and ultra-short solid-phase ion diffusion. This unique architecture enables Li-ion storage battery devices working with supercapacitor rate capabilities while maintaining high battery capacities. Our strategy paves a new way to fabricate free-standing binder-free electrode for high-performance electrochemical energy storage devices and is a significant step towards the development of the ultimate power source for next generation electric vehicles.

Acknowledgements

This work was financially supported by Chinese Ministry of Education in a framework of the Changjiang Scholar Innovative Research Team Program (IRT_15R52). This work is also supported by International Science & Technology Cooperation Program of China (2015DFE52870), Chinese Ministry of Education with a PhD Programs Foundation (20120143120019), Hubei Provincial Natural Science Foundation (2014CFB160), the National Science Foundation for Young Scholars of China (No. 51302204) and the Royal Academy of Engineering through a Fellowship (Graphlex). The authors also thank J. L. Xie, X. Q. Liu and T. T. Luo for TEM analysis from the Research and Test Center of Materials at Wuhan University of Technology.

Appendix A. Supporting Information

Materials characterizations and electrochemical characterizations.

References

[1] A. S. Aricò, P. Bruce, B. Scrosati, J. M. Tarascon, W. V. Schalkwijk, Nat. Mater. 4 (2005)

366-377.

[2] B. Kang , G. Ceder, Nature 458 (2009) 190-193.

[3] H. Zhang, X. Yu, P. V. Braun, Nat. Nanotech. 6 (2011) 277-281.

[4] J. Jiang, Y. Li, J. Liu, X. Huang, C. Yuan, X. W. Lou, Adv. Mater. 24 (2012) 5166-5180.

[5] Z. Gao, N. Song, X. Li, J. Mater. Chem. A, 3 (2015), 14833-14844.

[6] Z. Gao, W. Yang, J. Wang, N. Song, X. Li, Nano Energy 13 (2015) 306-317.

[7] M. V. Reddy, G. V. Subba Rao, B. V. R. Chowdari, Chem. Rev. 113 (2013) 5364-5457.

[8] A. Magasinski, P. Dixon, B. Hertzberg, A. Kvit, J. Ayala, G. Yushin, Nat. Mater. 9 (2010) 353-358.

[9] Y. Li, Z.Y. Fu, B. L. Su, Adv. Funct. Mater. 22 (2012) 4634-4667.

[10] D. Kong, J. Luo, Y. Wang, W. Ren, T. Yu, Y, Luo, Y. Yang, C. Cheng, Adv. Funct. Mater. 24 (2014) 3815-3826.

[11] D. H. Ha, M. A. Islam, R. D. Robinson, Nano Lett. 12 (2012) 5122-5130.

[12] Y. G. Guo, J. S. Hu, L. J. Wan, Adv. Mater. 20 (2008) 2878-2887.

[13] A. Vu, Y. Qian, A. Stein, Adv. Energy Mater. 2 (2012) 1056-1085.

[14] N. Feng, D. Hu, P. Wang, X. Sun, X. Li, D. He, Phys. Chem. Chem. Phys. 15 (2013) 9924-9930.

[15] C. Guan, X. Li, Z. Wang, X. Cao, C. Soci, H, Zhang, H. J. Fan, Adv. Mater. 24 (2012) 4186-4190.

[16] G. Zhang, X. W. Lou, Adv. Mater. 25 (2013) 976-979.

[17] X. Huang, H. Yu, J. Chen, Z. Lu, R. Yazami, H. H. Hng, Adv. Mater. 26 (2014)1296-1303.

[18] Z. Nie, A. Petukhova, E. Kumacheva, Nat. Nanotech. 5 (2010) 15-25.

[19] J. Lee, S. Zhang, S. Sun, Chem. Mater. 25 (2013) 1293-1304.

[20] X. Zheng, S. Yuan, Z. Tian, S. Yin, J. He, K. Liu, L. Liu, Mater. Lett. 63 (2009) 2283-2285.

[21] X. Zheng, S. Yuan, Z. Tian, S. Yin, J. He, K. Liu, L. Liu, Chem. Mater. 21 (2009) 4839-4845.

[22] X. Zheng, G. Shen, Y. Li, H. Duan, X. Yang, S. Huang, H. Wang, C. Wang, Z. Deng, B. L. Su, J. Mater. Chem. A 1 (2013) 1394-1400.

[23] B. Varghese, M. V. Reddy, Z. Yanwu, C. S. Lit, T. C. Hoong, G. V. S. Rao, B. V. R. Chowdari, A. T. S. Wee, C. T. Lim, C. H. Sow, Chem. Mater. 20 (2008) 3360-3367.

[24] V. Skumryev, S. Stoyanov, Y. Zhang, G. Hadjipanayis, D. Givord, J. Nogués, Nature 423 (2003) 850-853.

[25] Y. Li, X. Y. Yang, Y. Feng, Z. Y. Yuan, B. L. Su, Crit. Rev. Solid State Mat. Sci. 37 (2012) 1-74.

[26] Z. Nie, A. Petukhova, E. Kumacheva, Nat. Nanotech. 5 (2010) 15-25.

[27] S. Chabi, C. Peng, D. Hu, Y. Zhu, Adv. Mater. 26 (2014) 2440-2445.

[28] C. Wu, S. Deng, H. Wang, Y. Sun, J. Liu, H, Yan, ACS Appl. Mater. Interfaces 6 (2014) 1106-1112.

[29] S. P. Jahromi, A. Pandikumar, B. T. Goh, Y. S. Lim, W. J. Basirun, H. N. Lim, N. M. Huang, RSC Adv., 2015, 5, 14010

[30] F. I. Dar, K. R. Moonooswarmy, M. Es-Souni, Nanoscale Res. Lett. 8 (2013) 363.

[31] K. Liang, X. Tang, W. Hu, J. Mater. Chem. 22 (2012) 11062.

[32] F. Cao, G. X. Pan, X. H. Xia, P. S. Tang, H. F. Chen, Journal of Power Sources 264 (2014) 161-167.

[33] Q. Lu, M. W. Lattanzi, Y. Chen, X. Kou, W. Li, X. Fan, K. M. Unruh, J. G. Chen, J. Q. Xiao, Angew. Chem. Int. Ed. 50 (2011) 6847-6850.

[34] H. Yan, D. Zhang, J. Xu, Y. Lu, Y. Liu, K. Qiu, Y. Zhang, Y. Luo, Nanoscale Res. Lett. 9 (2014) 424.

[35] J. H. Pan, Q. Huang, Z. Y. Koh, D. Neo, X. Z. Wang, Q. Wang, ACS Appl. Mater. Interfaces 5 (2013) 6292-6299.

[36] S. J. Yang, S. Nam, T. Kim, J. H. Im, H. Jung, J. H. Kang, S. Wi, B. Park, C. R. Park, J. Am. Chem. Soc. 135 (2013) 7394-7397.

[37] J. M. Haag, G. Pattanaik, M. F. Durstock, Adv. Mater. 25 (2013) 3238-3243.

[38] L. Qie, W. M. Chen, Z. H. Wang, Q. G. Shao, X. Li, L. X. Yuan, X. L. Hu, W. X. Zhang, Y. H. Huang, Adv. Mater. 24 (2012) 2047-2050.

[39] H. Liu, G. Wang, J. Liu, S. Qiao, H. Ahn, J. Mater. Chem., 21 (2011) 3046.

[40] X. Wang, X. Li, X. Sun, F. Li, Q. Liu, Q. Wang, D. He, J. Mater. Chem., 21 (2011) 3571.

[41] V. Aravindan, P. S. Kumar, J. Sundaramurthy, W. C. Ling, S. Ramakrishna, S. Madhavi, Journal of Power Sources 227 (2013) 284-290.

[42]A. Caballero, L. Hernán, J. Morales, Z. González, A. J. Sánchez-Herencia, B. Ferrari, Energy Fuels 27 (2013) 5545-5551.

[43]C. Zhou, Y. Zhang, Y. Li, J. Liu, Nano Lett. 13 (2013) 2078-2085.

Xianfeng Zheng received his Ph.D. in Material Physics and Chemistry from Huazhong University of Science and Technology in 2010. Then, he started his postdoctoral researches at Wuhan University of Technology with Prof. Bao-Lian Su on hierarchically structured porous nanomaterials. Currently, he is an Assistant Professor in State Key Laboratory of Advanced Technology for Materials Synthesis and Processing from Wuhan University of Technology. His research interest is aimed at the bio-inspired design, synthesis and self-assembly of nanoparticles towards new nanomaterials with hierarchical porosity for energy and environment.

Hongen Wang received his Bachelor degree at Central South University in 2007 and Ph. D degree at City University of Hong Kong in 2012. He is now an Associate Professor in the Laboratory of Living Materials from the Wuhan University of Technology in 2012 and Postdoctoral Research Assistant in Physics and Materials Science at the City University of Hong Kong. His interests are mainly focused on the synthesis and applications of functional materials in the field of energy conversion and storage.

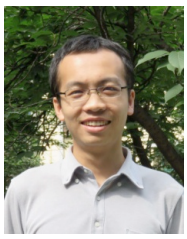

Chao Wang obtained his Master of Engineering degree in 2013 from Wuhan University of Technology, China. He is pursuing his Ph.D. degree under the guidance of Prof. Bao-Lian Su and Prof. Yu Li in Laboratory of Living Materials at State Key Laboratory of Advanced Technology for Materials Synthesis and Processing, Wuhan University of Technology, China. His current research involves developing techniques for advanced microscopy and the synthesis of organic-inorganic metal sulfide nanomaterials for photocatalysis applications and their antiphotocorrosion mechanism.

Zhao Deng received his B.S. and Ph.D. from Wuhan University of technology in 2005 and 2010. He worked as visiting scholar in CMI at the Universityof Namur with Prof. Bao-Lian Su in 2011. Currently, he works in Wuhan University of Technology. His research interests are synthesis of functional nanomaterials and their applications in catalysis, environmental protection and other fields.

Lihua Chen awarded his Ph.D degrees, one in inorganic chemistry from Jilin University, China (2009), and another in inorganic materials chemistry from University of Namur, FUNDP, Belgium (2011). In 2011-2012, he held a project-researcher position at the University of Namur with Professor Bao-Lian Su working on hierarchically porous zeolites. He is currently a full professor

working in the State Key Laboratory of Advanced Technology for Materials Synthesis and Processing from the Wuhan University of Technology, China. His research is aimed at new porous materials with designed hierarchically porosity towards catalysis.

Yu Li received his B.S. from Xi'an Jiaotong University in 1999 and received his M.S. from Liaoning Shihua University in 2002. He obtained his Ph.D. from Zhejiang University in 2005. He worked in EMAT at the University of Antwerp with Prof. G. Van Tendeloo in 2005 and then in CMI at the University of Namur with Prof. Bao-Lian Su in 2006. Currently, he is a "Chutian" professor at Wuhan University of Technology. His research interests include nanomaterials design and synthesis, hierarchically porous materials synthesis, and their applications in the fundamental aspects of energy and environment.

Tawfique Hasan gained his PhD from the University of Cambridge in 2009. He is currently a University Lecturer in Electronic Materials and Devices, Deputy Director for Teaching and Training of the EPSRC funded Centre for Doctoral Training in Graphene Technology and Director of the MRes program in Graphene Technology at the Cambridge Graphene Centre, Cambridge University Engineering Department. Hasan's current research focuses on formulation of functional inks of 0, 1- and 2-dimensional nanomaterials and their hybrids for a wide range of printable and flexible device applications including ultrafast lasers, photonic, (opto)electronic and energy devices. He is a Title A Fellow of Churchill College, Cambridge and currently holds a prestigious Royal Academy of Engineering Research Fellowship.

Prof. Bao-Lian Su created the Laboratory of Inorganic Materials Chemistry (CMI) at the University of Namur, Belgium in 1995. He is currently Full Professor of Chemistry, Member of the Royal Academy of Belgium, Fellow of the Royal Society of Chemistry, UK and Life Member of Clare Hall College, University of Cambridge. He is also Changjiang Professor at Wuhan University of Technology and an ‘‘Expert of the State’’ in the frame of ‘‘Thousands Talents’’ program, China. His current research fields include the synthesis, the property study and the molecular engineering of organized, hierarchically porous and bio-inspired materials, living materials and leaf-like materials and the immobilization of bio-organisms for artificial photosynthesis, (photo)Catalysis, Energy Conversion and Storage, Biotechnology, Cell therapy and Biomedical applications.

Supplementary Information

3D Interconnected Macro-mesoporous Electrode with Self-assembled NiO nanodots for High-performance Supercapacitor-like Li-ion Battery

Xianfeng Zheng[a], Hongen Wang[a], Chao Wang[a], Zhao Deng[a], Lihua Chen,[a] Yu Li,[a]* Tawfique Hasan[b] and Bao-Lian Su[a,c,d,]*

[a]*Laboratory of Living Materials at the State Key Laboratory of Advanced Technology for Materials Synthesis and Processing, Wuhan University of Technology, 122 Luoshi Road, 430070 Wuhan, Hubei, China; Email: yu.li@whut.edu.cn and baoliansu@whut.edu.cn*

[b]*Cambridge Graphene Centre, University of Cambridge, Cambridge, CB3 0FA, United Kingdom.*

[c]*Laboratory of Inorganic Materials Chemistry (CMI), University of Namur, 61 rue de Bruxelles, B-5000 Namur, Belgium; E-mail: bao-lian.su@unamur.be*

[d]*Department of Chemistry and Clare Hall College, University of Cambridge, UK; E-mail: bls26@cam.ac.uk*

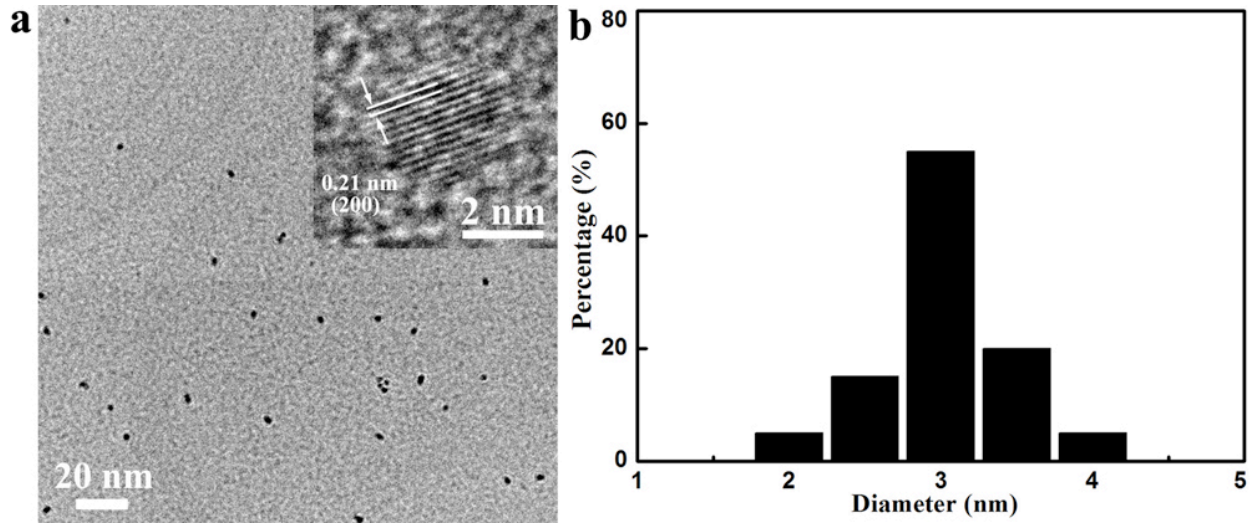

Figure S1. (a) TEM image of the monodispersed 3 nm NiO nanodots and inset showing the representative high-resolution TEM image of a single-crystalline NiO nanodot. (b) Histograms showing the distribution of particle-size measured by the TEM.

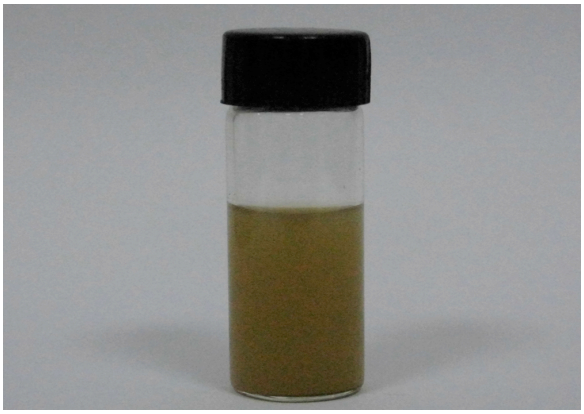

Figure S2. Photograph of as-synthesized 3 nm NiO nanodots highly dispersed in hexane for 6 months.

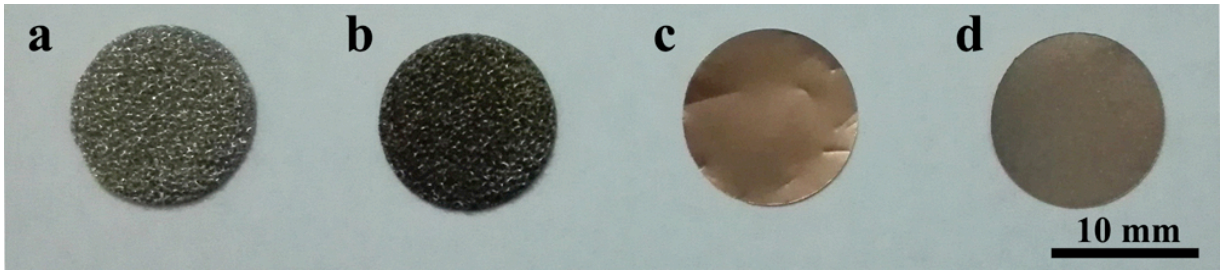

Figure S3. Photograph of (a) bare Ni foam (NF), (b) self-assembled 3 nm NiO nanodots on NF, (c) bare copper foil (CF) and (d) self-assembled 3 nm NiO nanodots on CF.

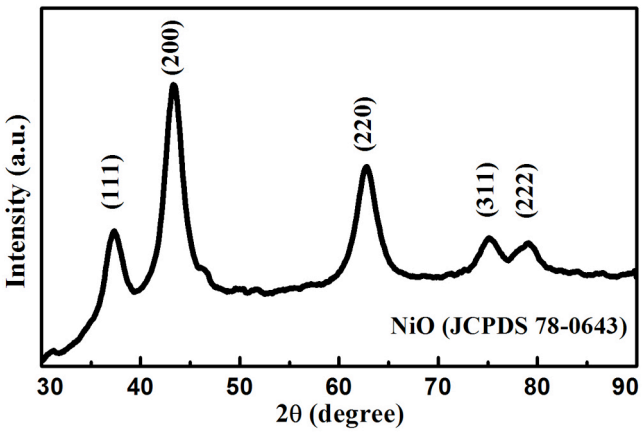

Figure S4. XRD patterns of the 3 nm NiO nanodots scraped from the substrate.

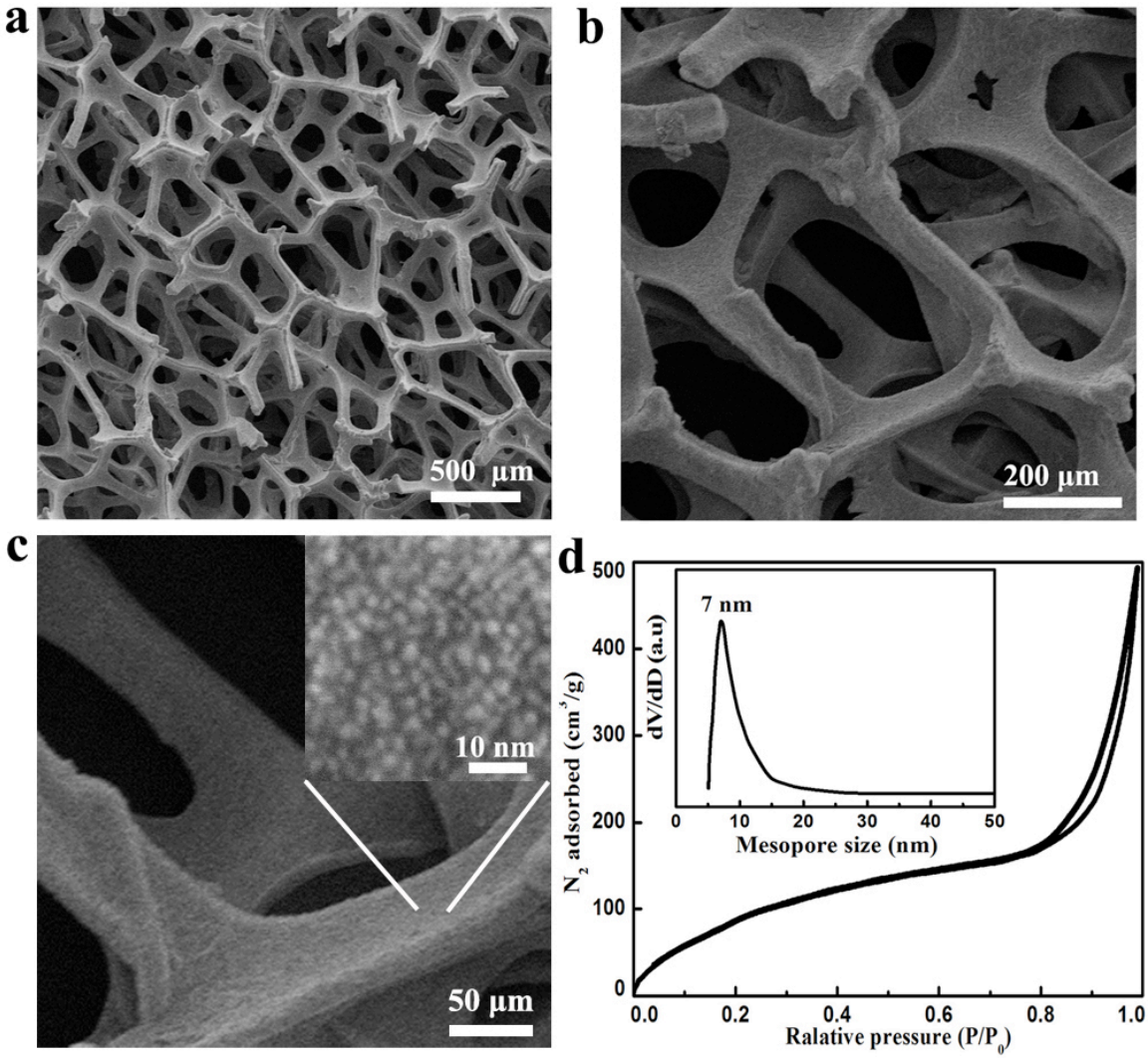

Figure S5. (a-c) SEM images of 3 nm NiO/NF. (d) N_2 adsorption-desorption isotherms of self-assembled 3 nm NiO nanodots scraped from the substrate. The inset shows the corresponding pore size distribution.

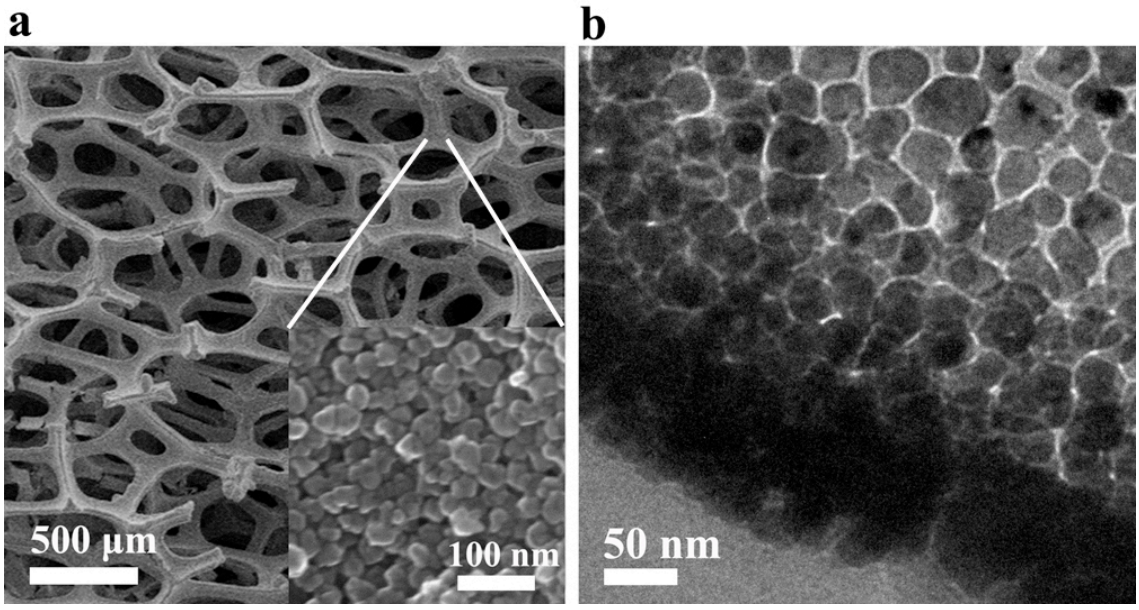

Figure S6. (a) SEM image and (b) TEM image of 30 nm NiO/NF. The inset in (a) clearly shows the self-assembled NiO nanoparticles.

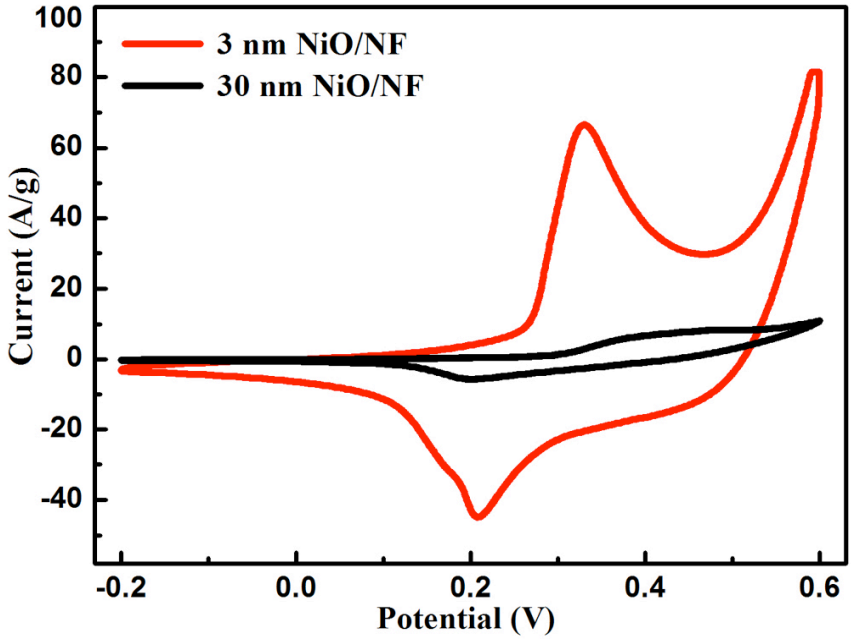

Figure S7. Cyclic voltammetry curves at scan rate of 100 mV s^{-1} for 3 nm NiO/NF and 30 nm NiO/NF as electrodes for supercapacitor, respectively.

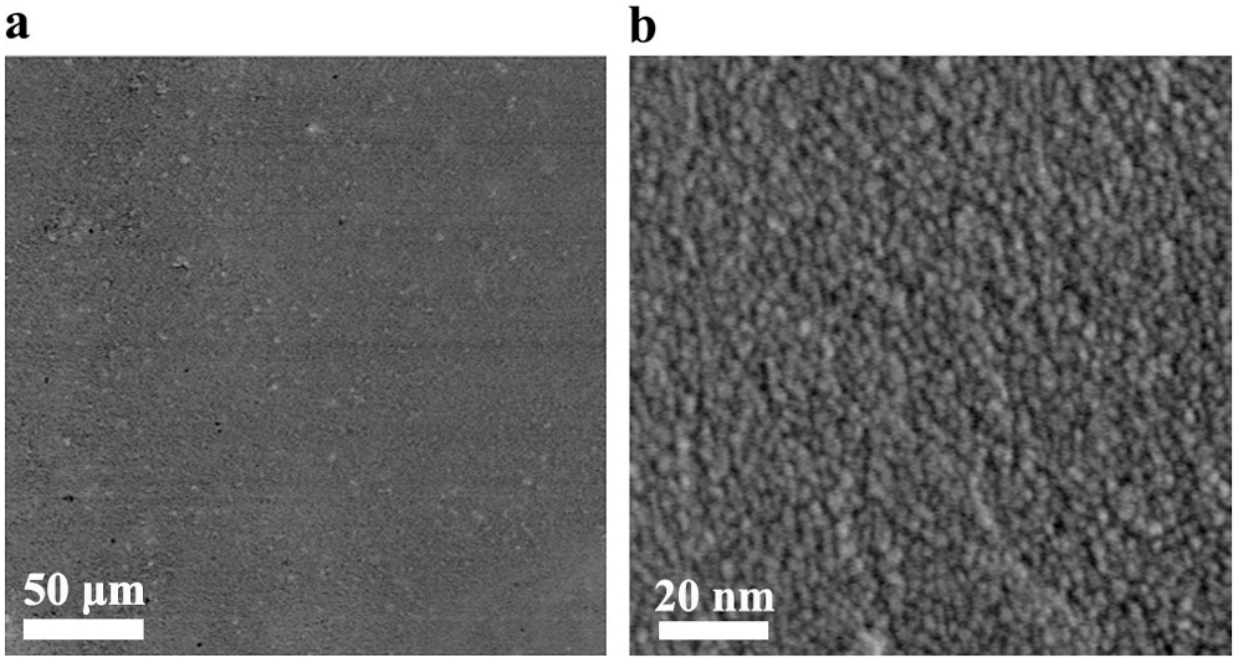

Figure S8. SEM images of 3 nm NiO/CF without macro-mesoporous structure with (a) low magnification and (b) high magnification.